ACSNANO

www.acsnano.org

ARTICLE

Cloaking Silica Nanoparticles with Functional Protein Coatings for Reduced Complement Activation and Cellular Uptake

Jae Hyeon Park, Joshua A. Jackman, Abdul Rahim Ferhan, Jason N. Belling, Natalia Mokrzecka, Paul S. Weiss,* and Nam-Joon Cho*

Cite This: *ACS Nano* 2020, 14, 11950−11961

Read Online

ACCESS | Metrics & More | Article Recommendations | Supporting Information

ABSTRACT: Silica-coated nanoparticles are widely used in biomedical applications such as theranostics, imaging, and drug delivery. While silica-coated nanoparticles are biocompatible, experimental evidence shows that they can trigger innate immune reactions, and a broader understanding of what types of reactions are caused and how to mitigate them is needed. Herein, we investigated how the noncovalent surface functionalization of silica nanoparticles with purified proteins can inhibit nanoparticle-induced complement activation and macrophage uptake, two of the most clinically relevant innate immune reactions related to nanomedicines. Silica nanoparticles were tested alone and after coating with bovine serum albumin, human serum albumin, fibrinogen, complement factor H (FH), or immunoglobulin G (IgG) proteins. Enzyme-linked immunosorbent assays measuring the generation of various complement activation products indicated that silica nanoparticles induce complement activation *via* the alternative pathway. All protein coatings other than IgG protected against complement activation to varying extents. Most proteins acted as steric blockers to inhibit complement protein deposition on the nanoparticle surface, while FH coatings were biologically active and inhibited a key step in the amplification loop of complement activation, as confirmed by Western blot analysis. Flow cytometry and fluorescence microscopy experiments further revealed that complement activation-inhibiting protein coatings blunted macrophage uptake as well. Taken together, our findings demonstrate a simple and effective way to coat silica nanoparticles with purified protein coatings in order to mitigate innate immune reactions. Such methods are readily scalable and might constitute a useful strategy for improving the immunological safety profile of silica and silica-coated nanoparticles as well as other types of inorganic nanoparticles.

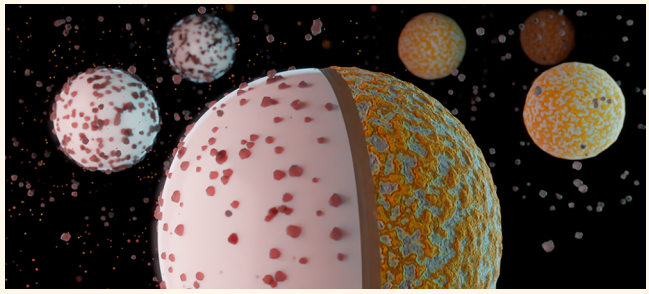

KEYWORDS: *nanoparticles, silica nanoparticles, silica-coated nanoparticles, complement activation, CARPA, cell uptake, innate immune response*

Silica nanoparticles and silica-coated nanoparticles (broadly defined as SiNPs) are widely used in biomedical applications such as theranostics, imaging, and drug delivery. They have many useful properties, including high biocompatibility, chemical stability in aqueous conditions, and ease of synthesis.[1−5] There are also a variety of methods to tailor the physicochemical properties of SiNPs, including nanoparticle size, porosity, shape, and surface chemistry.[6−8] Moreover, SiNPs have been deemed safe for human consumption by the U.S. Food and Drug Administration (FDA) and are incorporated into many consumer products such as cosmetics and food additives, from which they may be absorbed into the bloodstream.[9,10] Silica coatings are also important design components of biocompatible core−shell nanoparticles used intravenously, and the silica shell protects against oxidation and corrosion while minimizing cytotoxicity.[11−15] For example, quantum dots are often synthesized with a silica coating over the cadmium telluride (CdTe) or cadmium selenide (CdSe) nanocrystal core to reduce cytotoxicity without compromising optical features.[15,16] Similarly, a silica coating on magnetite (Fe_3O_4) and other magnetic nanoparticles also helps to minimize *in situ*

Received: June 18, 2020
Accepted: August 26, 2020
Published: August 26, 2020

https://dx.doi.org/10.1021/acsnano.0c05097
ACS Nano 2020, 14, 11950−11961

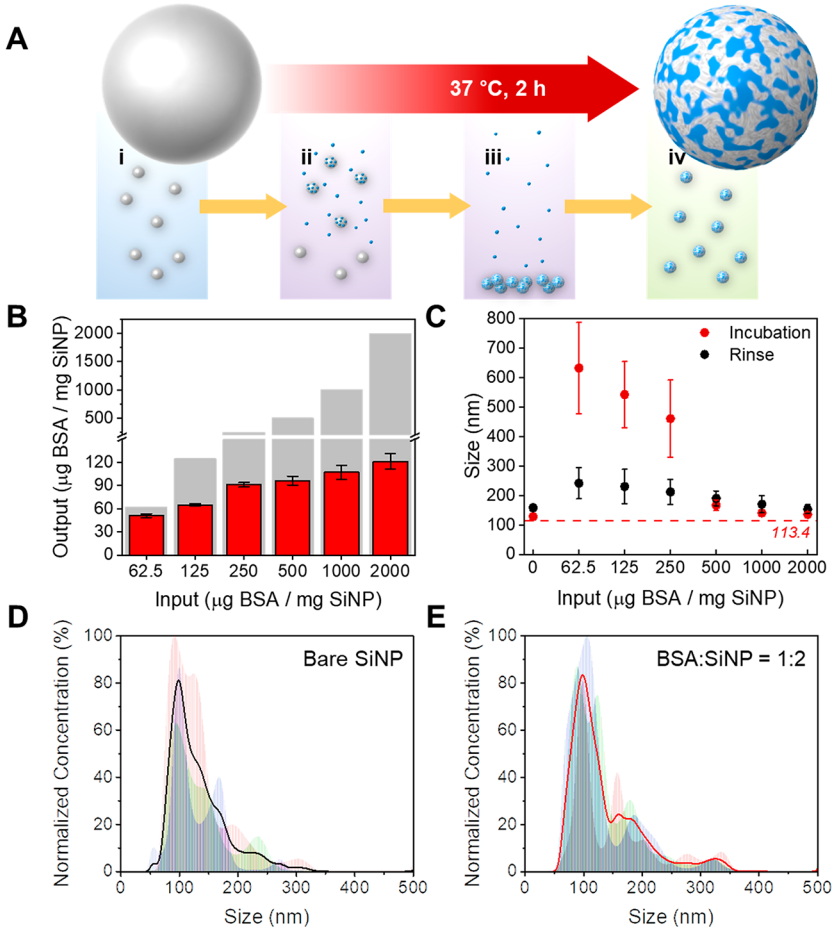

Figure 1. Schematic illustration of protein coating strategy and silica nanoparticle (SiNP) characterization. (A) SiNP coating protocol: (i) SiNPs were dispersed in aqueous buffer solution; (ii) they were mixed and incubated with protein solution at 37 °C for 2 h; (iii) they were centrifuged, and the SiNP pellet was collected, discarding the supernatant; and (iv) the pellet was resuspended in fresh buffer solution. Steps (iii) and (iv) were repeated a total of three times to prepare protein-coated SiNP sample. (B) Bicinchoninic acid (BCA) quantitative assay of surface-bound bovine serum albumin (BSA) on SiNPs (red) expressed as μg BSA per mg SiNP and the amount of BSA added to the initial mixture (gray), also expressed as μg BSA per mg SiNP. Data are reported as mean ± standard deviation (n = 3). (C) Intensity-weighted dynamic light scattering (DLS) characterization of BSA-coated SiNP size distribution (mean diameter) as a function of the BSA:SiNP mass ratio used in the coating protocol. The data are reported for after protein incubation with SiNPs (red) and after sample washing (black). The dashed line corresponds to the mean diameter of pristine SiNPs (~113.4 nm) and is presented for comparison. Data are reported as mean ± standard deviation (n = 3). Number-weighted nanoparticle tracking analysis (NTA) characterization of (D) pristine SiNPs and (E) BSA-coated SiNPs prepared using a 1:2 BSA:SiNP ratio. Bold line traces represent the average of n = 3 measurements.

degradation of the core, thereby prolonging usage for magnetic resonance imaging applications.[17−19]

At the same time, there is growing attention to SiNP interactions with immune system components, especially deleterious effects associated with intravenous administration such as cytokine storm and reactive oxygen species production.[20−22] The immune response level has also been shown to depend on the administered SiNP dose and physicochemical properties of the SiNP surface.[23,24] While there is growing awareness of these issues, there remains significant work ahead, especially in understanding how SiNPs might trigger complement activation, which is an innate immune response that occurs in blood in response to foreign nanoparticulates or microbes.[25] Complement activation begins with opsonic complement proteins binding to the target surface of foreign nanoparticulates in the bloodstream, and these binding events lead to a series of protein−protein interactions that trigger immune defense mechanisms.[26,27] Anaphylatoxins that are released as byproducts also attract macrophage immune cells, and opsonin-bound surfaces can be phagocytosed by macrophages.[28,29] Importantly, complement activation and related uptake processes can lead to adverse immune responses such as hypersensitivity reactions known as complement activation-related pseudoallergy (CARPA), which is a serious side effect of numerous nanomedicines, biologicals, and imaging agents that can lead to severe illness or even death.[30−33] Long-term outcomes of aberrant complement activation can also include chronic inflammation, leading to diseases such as rheumatoid arthritis or vasculitis.

The critical initiation steps of complement activation involve the binding of complement proteins to foreign nanoparticulate surfaces, and thus there is interest in developing nanomaterial surface modification strategies that prevent complement protein adsorption through steric blocking. This stealth strategy typically involves cloaking nanoparticles with a bioinert, thin film coating such as hydrophilic poly(ethylene glycol) (PEG) brushes, which have been widely used to prevent protein adsorption[34,35] and work well with SiNPs.[36−38]

https://dx.doi.org/10.1021/acsnano.0c05097
ACS Nano 2020, 14, 11950−11961

For example, He *et al.* showed that PEG-coated SiNPs could effectively reduce nonspecific binding of human serum albumin from 18.7% to 2.5% along with decreasing macrophage uptake efficiency *in vitro* from 8.6% to 0.1%.[39] However, there is mounting evidence that PEG coatings can cause adverse immune effects due to incomplete blocking of complement protein adsorption[40] and/or due to the presence of pre-existing anti-PEG antibodies.[41] A classic example is the PEG-functionalized Doxil liposomal formulation that has been reported to be a CARPA activator.[40,42,43] In light of these considerations, there has been active exploration of cloaking nanoparticles with alternative types of stealth coatings, including cellular membrane extracts (*e.g.*, erythrocytes) and purified proteins.[44−47] The development of protein-based coatings that are preadsorbed onto the nanoparticles before exposure to physiological fluids is particularly useful because the coating can have multiple functions; these include not only steric blocking effects but also biological functions depending on protein conformation(s) in the adsorbed state.[48−50] Indeed, even after a protein corona forms on the outer nanoparticle surface in physiological fluids, the preadsorbed proteins can remain partially exposed and retain functional properties, in some cases.[51−54] Thus, it is imperative to understand the risk potential of SiNPs for triggering complement activation and to develop preemptive protein coating-based strategies to mitigate not only complement activation but also related innate immune responses such as macrophage uptake.

Herein, we demonstrate a simple and effective strategy to coat SiNPs with noncovalently adsorbed protein coatings in order to attenuate complement activation and to protect against macrophage uptake. While most protein-based coatings involve steric blocking alone, a key aspect of our biofunctionalization strategy is to explore functional proteins that have been implicated in regulating different parts of complement activation and to devise methods that endow SiNPs with the immunomodulatory functions of the coated protein. Our study begins with optimizing the coating protocol to form a tightly bound layer of adsorbed protein molecules on the SiNP surface based on quantification of adsorbed protein quantity on SiNP surfaces along with nanoparticle size characterization. The optimized coating approach is then applied to coat SiNPs with various classes of proteins, including steric blockers such as bovine serum albumin (BSA) and human serum albumin (HSA), complement inhibitors such as fibrinogen (FIB) and factor H (FH), and immune-stimulating proteins such as immunoglobulin G (IgG). Notably, HSA, IgG, and FIB are among the most abundant proteins in human blood plasma, with each accounting for around 55%, 38%, and 7% of total plasma proteins, respectively, and their high abundance makes them suitable options for nanoparticle coating applications. Enzyme-linked immunosorbent assay (ELISA) and Western blot experiments enabled us to elucidate the mechanistic details of how SiNPs induce complement activation and to identify how protein coatings can mitigate complement activation. The most pronounced effects occurred with protein coatings that not only sterically blocked complement proteins from adsorbing onto SiNP surfaces but also retained suitable functional properties on the SiNP surface and played active roles in inhibiting key processes in the complement activation cascade. Importantly, protein coatings that were effective at inhibiting complement activation also decreased macrophage uptake efficiency. Taken together, the findings in this work demonstrate a broadly versatile approach to improve the immunological profile of SiNPs, and the approach can be extended to a wide range of silica and silica-coated nanoparticles for various applications along with other types of inorganic nanoparticles.

RESULTS AND DISCUSSION

Protein Coatings on Silica Nanoparticles. We begin by establishing a versatile strategy to coat protein adlayers on SiNPs and thereby understand how incorporating various proteins such as BSA, HSA, FIB, FH, and IgG can modulate innate immune responses in a controlled manner. Toward this goal, a well-packed monolayer of noncovalently adsorbed protein molecules was formed on the SiNP surface through precise adjustment of ionic strength and temperature during a solution-phase incubation step in order to enhance protein−surface interactions and the extent of surface-induced protein denaturation,[55,56] resulting in a simple and effective protein coating protocol[45] (Figure 1A). In brief, SiNPs with a hydrodynamic diameter of *ca.* 112 nm were incubated with an aqueous protein solution for 2 h at 37 °C, followed by extensive washing to remove weakly adsorbed proteins as well as residual proteins in solution. Only irreversibly adsorbed protein molecules on the SiNP surface (akin to the hard corona that forms in biological systems) that remained bound after three washings were quantified by a bicinchoninic acid (BCA) protein assay in addition to dynamic light scattering (DLS) and nanoparticle tracking analysis (NTA) characterization of the nanoparticle size distribution before and after protein coating.

To optimize the coating protocol, BSA was used as a model protein and was incubated with SiNPs across a range of mass ratios from 1:16 to 2:1 BSA:SiNP. With increasing BSA fraction, the amount of surface-bound BSA increased from 50 to 120 μg BSA per mg SiNP (Figure 1B). This range agrees with past literature on silica-coated magnetic iron oxide nanoparticles that estimated a saturation value of 85 μg of BSA per 1 mg of nanoparticles.[57] Saturation of adsorbed BSA on the SiNPs occurred from a 1:4 BSA:SiNP mass ratio, while there was incomplete surface coverage of adsorbed proteins at lower mass ratios.[58] Intensity-weighted DLS experiments revealed that BSA-coated SiNPs were more prone to aggregate at low BSA:SiNP ratios,[59] as indicated in Figure 1C. The pristine SiNPs resuspended in buffer solution had a hydrodynamic diameter of 113 nm, while the aggregated ones reached as large as *ca.* 600 and 250 nm before and after washing, respectively. At 1:2 and higher BSA:SiNP ratios, the colloidal stability of BSA-coated SiNPs was greatly improved and nanoparticle sizes became consistent with the expected size of pristine SiNPs with an additional protein adlayer. The colloidal stability of the nanoparticle suspensions was verified by number-weighted NTA experiments, which is more sensitive to capturing the full size distribution of protein-coated nanoparticles in suspension.[60,61] Both pristine SiNPs and BSA-coated SiNPs prepared using a 1:2 BSA:SiNP mass ratio had narrow size distributions with median diameters around 117 and 119 nm, respectively (Figure 1D,E). Thus, a mass ratio of 1:2 protein:SiNP was chosen for preparing protein-coated SiNPs based on effective protein consumption and high colloidal stability. Table S1 presents the characterization data for each type of protein, and all were able to form stable protein-coated SiNP suspensions except for IgG, which caused moderate nanoparticle aggregation, as previously reported.[62]

https://dx.doi.org/10.1021/acsnano.0c05097
ACS Nano 2020, 14, 11950−11961

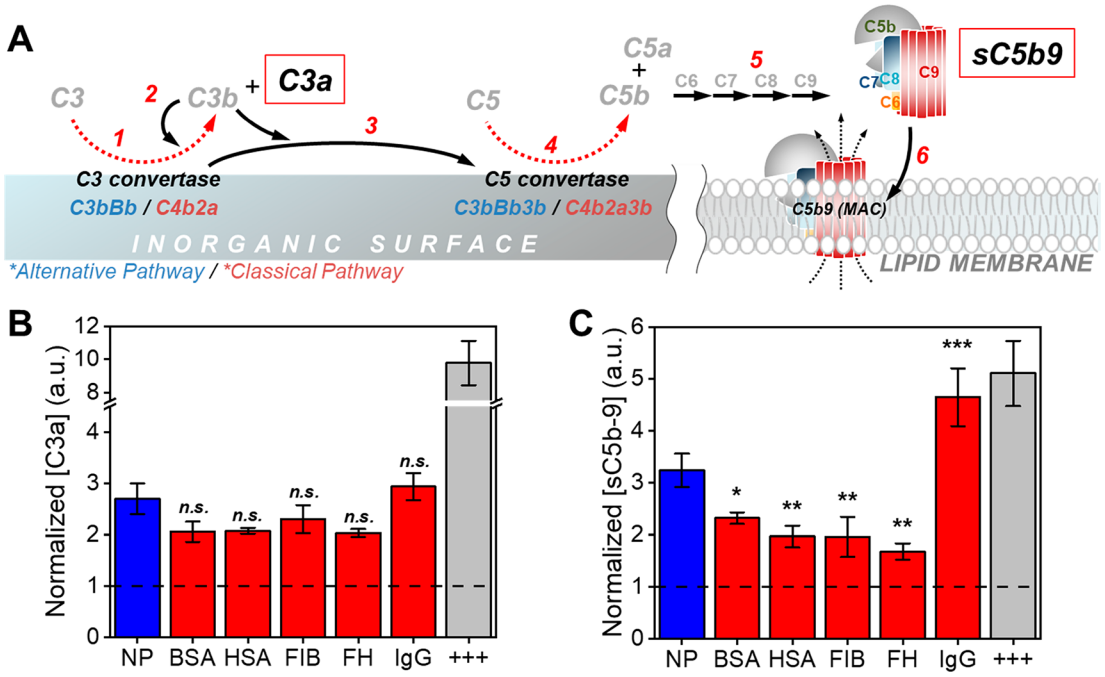

Figure 2. Evaluation of total complement activation triggered by pristine and protein-coated silica nanoparticles (SiNPs). (A) Schematic illustration of complement activation cascade on nanoparticle surface triggered by the alternative pathway (AP) (blue) or the classical pathway (CP) (red). The basic steps include the following: (1) Proteolytic activity of C3 convertase cleaves and activates complement C3 protein into C3b while releasing an anaphylatoxin, C3a; (2) activated C3b adsorbs onto ("opsonizes") the nanoparticle surface and binds with factor B to form the C3 convertase (C3bBb), which completes the amplification loop; (3) alternatively, C3b can bind to another C3 convertase (C3bBb or C4b2a) to form the C5 convertase (C3bBb3b or C4b2a3b); (4) C5 is cleaved by the C5 convertase to generate a secondary anaphylatoxin, C5a, and an active C5b fragment; (5) terminal complement pathway is initiated by the C5b fragment to assemble the membrane attack complex (MAC) that also includes complement C6, C7, C8, and multiple C9 proteins; and (6) the assembly of MAC (also known as sC5b-9 in soluble form) on cellular membranes can cause pore formation and membrane lysis. Enzyme-linked immunosorbent assay (ELISA) results show (B) C3a concentrations and (C) sC5b-9 concentrations produced due to incubation in normal human serum (NHS) with pristine SiNPs (blue) or protein-coated SiNPs (red). The positive control (gray) is established with heat-denatured IgG (denoted by +++ symbols). The reported concentrations are normalized to baseline levels in NHS without SiNPs, as indicated by the dashed line in each graph. Data are reported as mean ± standard deviation ($n = 9$). Statistical significance was analyzed by one-way ANOVA with Tukey's test and indicated by n.s. ($p \geq 0.05$), * ($p < 0.05$), ** ($p < 0.005$), or * ($p < 0.0005$).**

Modulation of Silica Nanoparticle-Triggered Complement Activation. Complement activation is an innate immune response that can be triggered by one or more of three activation pathways: the classical pathway (CP), the lectin pathway (LP), and the alternative pathway (AP). The CP is initiated upon recognizing immunoglobulin isotopes, while the LP is triggered by the binding of mannan-binding lectin (MBL) onto glycoproteins or other carbohydrate molecules often present on microbial surfaces.[63,64] On the other hand, the AP starts from the spontaneous conversion of the complement C3 protein into a hydrolyzed C3(H_2O) form, which initiates the cascade of complement protein−protein interactions. Each pathway involves the sequential assembly of the C3 convertase and C5 convertase, which subsequently triggers the terminal release of a potent toxin called C5b-9 (or sC5b-9 in its soluble form), which is also known as the membrane attack complex (MAC) (Figure 2A). Thus, measuring the byproducts of C3 convertase and C5 convertase activity relative to baseline levels in normal human serum (NHS) provides insight into the degree of total complement activation across all three pathways.[65]

In our experiments, we measured the degree of complement activation caused by SiNPs and the extent to which protein coatings could protect against complement activation. Pristine and protein-coated SiNPs were incubated with NHS, and then ELISA experiments were conducted to measure C3a and sC5b-9 generation as indicators of C3 and C5 convertase activity, respectively. Figure 2B presents the measured levels of C3a marker, and pristine SiNPs triggered a 2.7-fold increase from NHS baseline levels. All protein-precoated SiNPs, except for IgG-coated SiNPs, tended to decrease C3a levels but without statistical significance. On the other hand, IgG-coated SiNPs induced comparable or slightly higher levels of C3a as compared to the pristine nanoparticles. More significant effects were observed in the sC5b-9 assay, as shown in Figure 2C. Pristine SiNPs caused a 3.2-fold increase compared to baseline levels in NHS without SiNPs. Meanwhile, BSA, HSA, and FIB coatings decreased SiNP-induced complement activation by *ca.* 25 to 40% reductions, likely by virtue of steric blocking effects. On the other hand, FH coatings had a more significant effect, with over 50% protection against complement activation, which suggests that adsorbed FH may retain functional activity, specifically its ability to inactivate C3b and thus inhibit C3 and C5 convertases.[66]

Evaluation of Complement Activation Pathways. To gain mechanistic insight into how different protein coatings modulate SiNP-triggered complement activation levels, we performed additional ELISA experiments under conditions in which only CP/LP or AP pathways were active. We first studied the AP pathway by adding 10 mM Mg-EGTA to NHS

https://dx.doi.org/10.1021/acsnano.0c05097
ACS Nano 2020, 14, 11950−11961

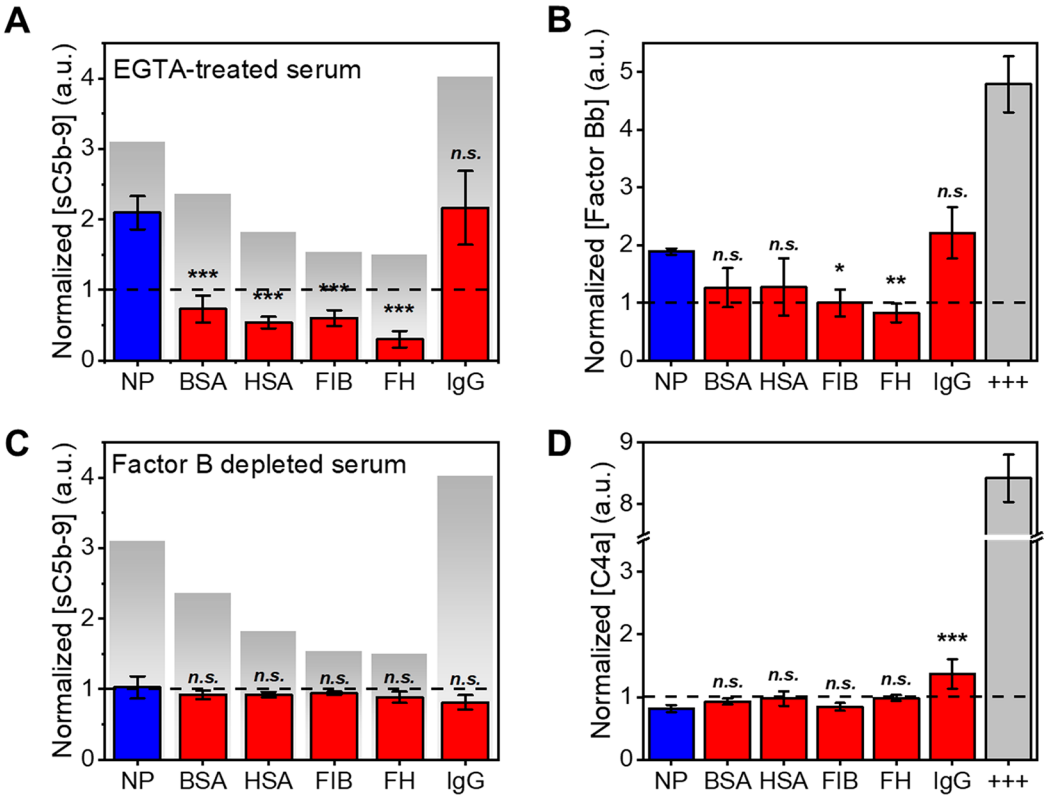

Figure 3. Decoupling silica nanoparticle (SiNP)-triggered complement activation effects across alternative and classical pathways. Alternative pathway (AP)-related enzyme-linked immunosorbent assay (ELISA) results for the following markers: (A) sC5b-9 concentrations in ethylene glycol-bis(2-aminoethyl ether)-*N,N,N′,N′*-tetraacetic acid (EGTA)-treated serum and (B) Bb production in normal human serum (NHS) after incubation with pristine SiNPs (blue) or protein-coated SiNPs (red). Classical pathway (CP)-related ELISA results for the following markers: (C) sC5b-9 concentrations in Factor B-depleted serum and (D) C4a production in NHS after incubation with pristine SiNPs (blue) or protein-coated SiNPs (red). The reported concentrations are normalized to baseline levels in NHS without SiNPs, as indicated by the dashed line in each graph. Data are reported as mean ± standard deviation ($n = 9$). Statistical significance was analyzed by one-way ANOVA with Tukey's test and indicated by n.s. ($p \geq 0.05$), * ($p < 0.05$), ** ($p < 0.005$), or * ($p < 0.0005$). For the sC5b-9 data sets in panels (A) and (C), the corresponding data in NHS (*cf.* Figure 2) are superimposed in the background for comparison. In panels (B) and (D), the positive control (gray) is established with heat-denatured IgG (denoted by +++ symbols).**

(EGTA = ethylene glycolbis(2-aminoethyl ether)-*N,N,N′,N′*-tetraacetic acid), which inhibited C1q assembly, a prerequisite for CP initiation,[67] and then measured sC5b-9 generation (Figure 3A). Pristine SiNPs triggered a 2.1-fold increase of sC5b-9 compared to baseline levels of untreated NHS, and BSA, HSA, FIB, and FH coatings all suppressed sC5b-9 generation below this baseline level. Matching earlier trends, the detected concentration of sC5b-9 increased in response to the IgG coating. In a separate experiment, we measured the level of complement factor Bb generated in SiNP-spiked NHS (Figure 3B). Once again, similar trends were observed whereby pristine SiNPs increased Bb production compared to the baseline levels in NHS, BSA and HSA coatings tended to decrease Bb production levels, FIB and FH coatings significantly decreased Bb production levels, and IgG coatings increased Bb production.

We also studied the CP pathway by using Factor B-depleted serum in which the AP pathway is inactive. Strikingly, pristine SiNPs did not induce complement activation along the classical pathway and the protein coatings also had negligible effects compared to baseline levels (Figure 3C). In addition, we measured generation of complement C4a protein in NHS, which is another byproduct related to the classical pathway, and generally observed negligible effects of pristine and protein-coated SiNPs on this marker compared to baseline levels (Figure 3D).[68] The only exception was IgG-coated SiNPs, which caused an increase in C4a level, which is consistent with the role of IgG as a known trigger of the classical pathway. Taken together, these data are all consistent with SiNPs inducing complement activation primarily along the AP pathway and modulatory activities of protein coatings being related to steric blocking and/or interactions with AP-related protein components.

Unraveling Functional Properties of Protein Coatings. The protective effects of protein coatings against SiNP-induced complement activation led us to investigate whether the protein coatings passively inhibit complement activation through steric blocking or play more active roles in blunting specific steps in complement activation. For example, FH is known to play an important role in the AP pathway, where it can inactivate C3b protein, while FIB can inhibit the CP pathway.[69] In contrast, serum albumins such as BSA and HSA are used as dysopsonins to prevent plasma adsorption by steric blocking effects.[49] Within this scope, it is important to point out that soluble proteins and adsorbed proteins typically exhibit different conformations[70] and, thus, potentially altered molecular functions, which led us to investigate whether SiNP-bound FH could still inactivate C3b (as soluble FH does) along with testing other selected proteins for comparison. Our experimental design was premised on the important role that

https://dx.doi.org/10.1021/acsnano.0c05097
ACS Nano 2020, 14, 11950−11961

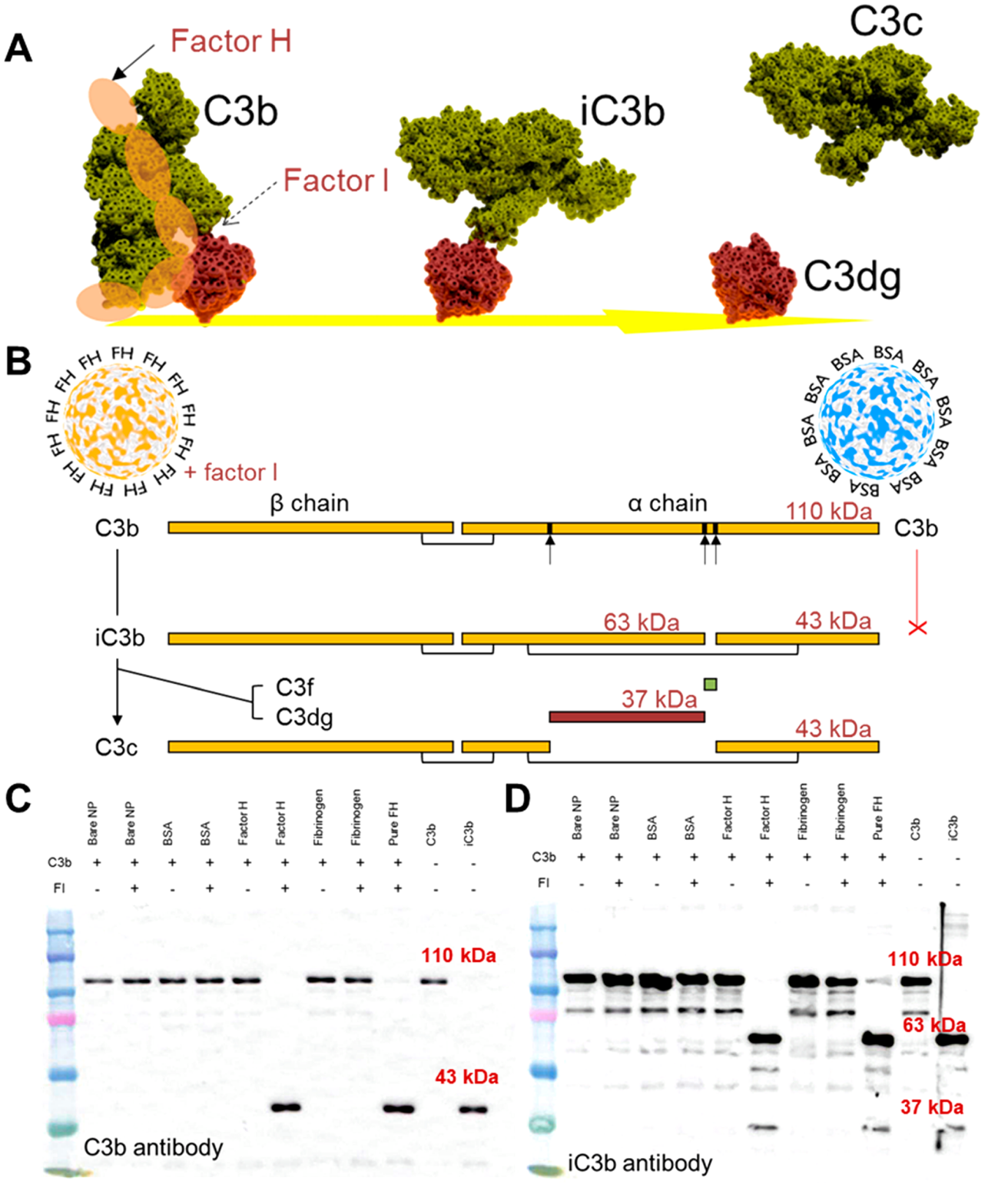

Figure 4. Western blot analysis of C3b cleavage by protein-coated silica nanoparticles (SiNPs). (A) Factor H interacts with C3b protein, and this interaction is necessary for factor I to cleave C3b into iC3b, which can then break down to release C3c (dark yellow) while leaving C3dg surface-bound (red). (B) Step-by-step cleavage of C3b protein into iC3b protein, followed by breakdown into C3c, C3dg, and C3f products. A simplified model of the multidomain C3b structure is depicted with disulfide bridges and the cleavage sites indicated by the arrows. The multidomain C3b protein has α- and β-chains; however, it is fully reduced in the electrophoretic gel environment such that the α- and β-chains are separate. Pristine and protein-coated SiNPs along with various controls were incubated with normal human serum (NHS) in the presence or absence of purified factor I, and C3b cleavage was evaluated by Western blot analysis. The blot results are shown for (C) C3b and (D) iC3b antibody stains.

https://dx.doi.org/10.1021/acsnano.0c05097
ACS Nano 2020, 14, 11950−11961

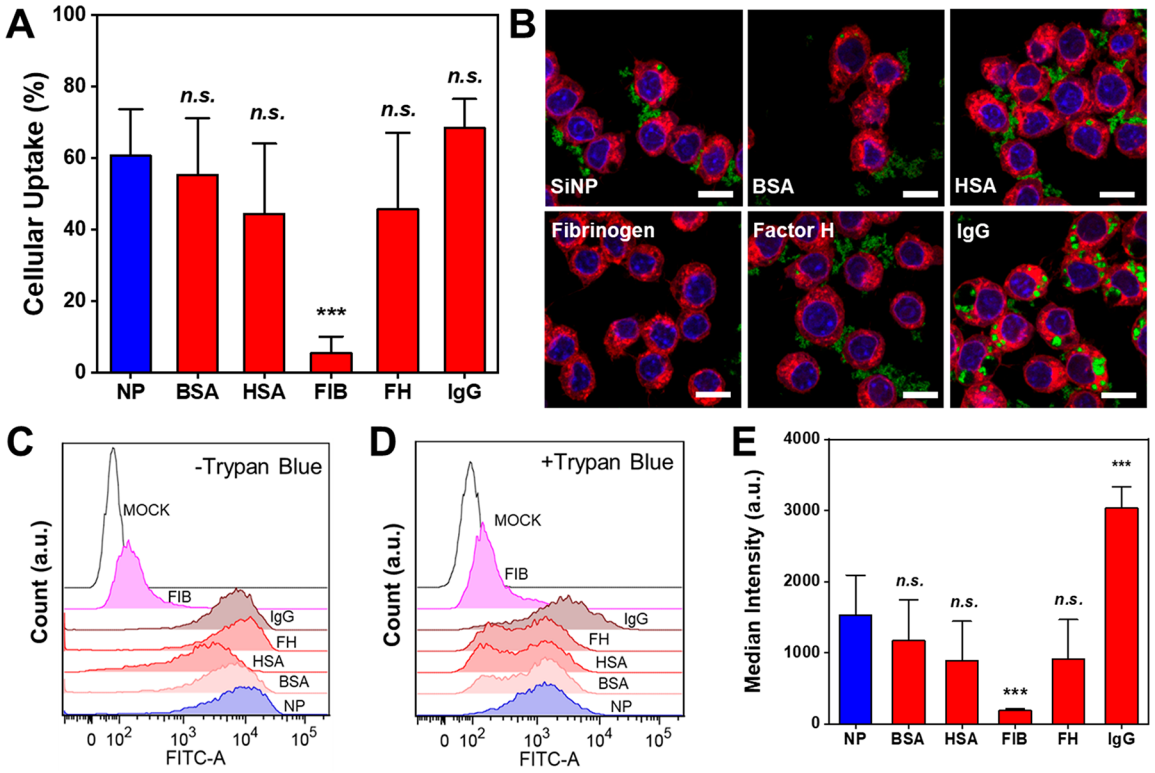

Figure 5. Flow cytometry analysis and confocal microscopy imaging of protein-coated silica nanoparticle (SiNP) uptake by macrophage cells. (A) Flow cytometry (FCM) results of cell uptake efficiency calculated by the percentage of individual cells emitting a threshold FITC signal relative to the total number of cells. Data are reported as mean ± standard deviation (n = 5). Statistical significance was analyzed by one-way ANOVA with Tukey's test. and indicated by n.s. ($p \geq 0.05$), * ($p < 0.05$), ** ($p < 0.005$), or * ($p < 0.0005$). (B) Confocal laser scanning microscopy images of RAW264.7 cells with 4′,6-diamidino-2-phenylindole (DAPI)-stained cell nuclei (blue) and CellMask Orange-stained cellular membranes (red) after treatment with fluorescein isothiocyanate (FITC)-labeled pristine and protein-coated SiNPs (green). Scale bars: 10 μm. Histogram overlay plots of flow cytometry (FCM) analysis show the distribution of FITC intensity values (C) before and (D) after fluorescent quenching with Trypan blue (TB). (E) Median fluorescence intensity of FITC after treating each batch of cells (10 000 cells per sample) with TB. Data are reported as mean ± standard deviation (n = 5). Statistical significance was analyzed by one-way ANOVA with Tukey's test and indicated by n.s. ($p \geq 0.05$), * ($p < 0.05$), ** ($p < 0.005$), or *** ($p < 0.0005$).**

the AP plays in SiNP-induced complement activation, the high inhibitory effects of FH coatings observed in our SiNP experiments, insights from other case studies of functional protein precoatings,[53] and the potential implications of molecular conformation to maintain the functional activity of FH.[71]

Biologically, factor I (FI) is the protease that cleaves C3b into iC3b, but FI is only active when FH is present as the cofactor. Thus, iC3b along with other byproducts (C3c/C3dg) can be detected if FI and FH are present and functional (Figure 4A). When the C3b protein is cleaved, the ∼110 kDa α-chain of C3b is cleaved into two α-subchains that are linked by a disulfide bond, and they weigh ∼43 and ∼63 kDa, respectively. In addition, the larger 63 kDa α-subchain can be cleaved into a ∼37 kDa subfragment, which is C3dg that remains anchored to the surface while releasing the rest of the subfragment along with a secondary α-subchain that is linked through the disulfide bond and is altogether known as C3c (Figure 4B).

Experimentally, we performed a cofactor assay to determine if different protein coatings on SiNPs could interact with and trigger the cleavage of purified, solution-phase C3b protein, as determined by Western blot analysis. Briefly, BSA-coated, FIB-coated, and FH-coated SiNPs were incubated with C3b, either with or without factor I, and we measured whether the protein-coated SiNPs could inactivate C3b protein. Figure 4C presents the Western blot data obtained with C3b antibody staining. Pristine SiNPs along with BSA- and FIB-coated SiNPs did not cleave C3b, as indicated by a single band belonging to the ∼110 kDa α-chain of C3b. On the other hand, FH-coated SiNPs and soluble FH by itself both cleaved C3b, resulting in iC3b formation. As a result, there was only one band present around ∼43 kDa, which is the band observed for purified iC3b alone and consistent with the cleaved ∼43 kDa α-subchain of C3b. These findings were confirmed by additional Western blot experiments with iC3b antibody staining, which showed that only FH-coated SiNPs and soluble FH are functionally active (Figure 4D). Specifically, the observed bands were located at ∼63 and ∼37 kDa and correspond to the other cleaved α-subchain of C3b along with a subfragment thereof, respectively. These data confirm that FH-coated SiNPs are functionally active to inhibit an important step in the alternative pathway of complement activation, while BSA- and FIB-coated SiNPs did not inhibit this step.

Effects on Macrophage Uptake. The immediate biological response to nanoparticles *in vivo* is the rapid accumulation of proteins, including complement proteins and other immune-activating opsonins, on the nanoparticle surface that adhere as a result of the nanoparticles' high surface energies and form the coronas. Surface receptors of macrophages such as Toll-like receptors, mannose receptors, scavenger receptors, and Fc receptors interact with the protein

https://dx.doi.org/10.1021/acsnano.0c05097
ACS Nano 2020, 14, 11950−11961

corona and facilitate nanoparticle uptake by either phagocytosis or endocytosis.[72] In particular, complement proteins and IgG accelerate macrophage uptake by phagocytosis, as mediated by complement receptors and Fc receptors, respectively.[73] On the other hand, pristine SiNPs in serum-free media are also internalized by macrophages in a process that is driven by the intrinsic surface energies of the nanoparticles and through receptor-mediated mechanisms.[74] In such cases, the uptake of pristine SiNPs has been reported to cause cellular toxicity in a dose-dependent manner.[24] Hence, protein precoatings on the SiNP surface can potentially mitigate both cellular toxicity as well as complement activation *via* steric blocking and/or active complement regulation, including preventing or at least diminishing macrophage uptake.

Accordingly, we incubated pristine and protein-coated SiNPs with RAW 264.7 murine macrophages and measured cell uptake levels (Table S2). For these experiments, fluorescein isothiocyanate (FITC)-labeled SiNPs were used for imaging purposes. After incubation, cells were sorted by flow cytometry (FCM) and revealed that *ca.* 60% of macrophages emitted a FITC fluorescence signal indicative of SiNP uptake when treated with pristine SiNPs, while comparable results were observed with BSA- and IgG-coated SiNPs (Figures 5A and S1). There was a tendency toward lower uptake of HSA- and FH-coated SiNPs, but without statistical significance, while less than 10% of macrophages exhibited uptake of FIB-coated SiNPs. Confocal laser scanning microscopy (CLSM) imaging experiments were also performed to visualize SiNP uptake (Figures 5B and S2). Pristine SiNPs mainly accumulated on the cell surface along with BSA-, HSA-, and FH-coated SiNPs, whereas a smaller fraction of SiNPs was internalized within the cells. On the other hand, negligible uptake was observed for FIB-coated SiNPs. There was also pronounced cell uptake of IgG-SiNPs, including extensive internalization due to phagocytosis. Similar observations have been reported in the case of γ-globulin coatings[75] and demonstrate that functional protein coatings can modulate not only complement activation but also macrophage uptake.

Histogram of FITC signal intensity values analyzed by FCM further revealed the distribution of attached SiNPs per cell, accounting for both cell surface-adsorbed SiNPs *and* phagocytosed SiNPs (Figure 5C). The measured trends indicated relatively high uptake levels for IgG- and FH-coated SiNPs, while BSA- and HSA-coated SiNPs tended to have modestly lower levels than pristine SiNPs, and FIB-coated SiNPs had negligible uptake. To distinguish the intracellular localization of FITC-SiNPs from those that adhere to the extracellular cell membrane, we treated cellular samples with Trypan blue (TB) in order to quench the fluorescence of cell surface-adsorbed SiNPs so that any detected FITC signal belonged only to phagocytosed SiNPs (Figures 5D, S3, and S4). In this case, a new subpopulation emerged from the histograms of BSA-, HSA-, and FH-coated SiNPs in a fluorescent intensity range that was equivalent to the background noise and indicated that a large fraction of cells was unable to internalize surface-adsorbed SiNPs.[74] The staggered macrophage response suggests that the protein coatings impede pattern recognition by cell surface receptors.[72] Meanwhile, the FITC signal intensity for all cellular samples decreased nearly 10-fold, on average. The median intensity of each cellular sample after TB treatment was compared to summarize the phagocytosis profile of the different SiNP preparations (Figure 5E). The results indicate that FH coatings also inhibited cell uptake, although FH-coated SiNPs can adhere to macrophage cell surfaces. In contrast, there were still high FITC signals for IgG-coated SiNPs even after TB treatment, indicating that IgG-coated SiNPs were mainly phagocytosed. There was again low uptake of FIB-coated SiNPs; notably, the FIB-coated SiNPs were more prone to aggregation than other protein-coated SiNPs as discussed above albeit still within the size range of particles amenable to phagocytosis (<6 μm; see ref 72). Overall, the cell uptake results demonstrate the importance of the protein coatings themselves as functional elements in the nanoparticle design that can modulate both complement activation and macrograph uptake.

CONCLUSIONS AND PROSPECTS

In this work, we have demonstrated that noncovalently adsorbed protein coatings on SiNPs can mitigate complement activation as well as decrease the extent of macrophage uptake. While some steric-blocking proteins performed well to facilitate dysopsonization of complement proteins (*i.e.*, BSA, HSA, and FIB), the incorporation of immune-regulating proteins such as FH resulted in more optimal performance on account of steric blocking effects *and* active complement inhibition. Furthermore, the protein coatings were able to effectively cloak the pristine nanoparticle surface in order to avoid recognition by macrophage surface receptors and to prevent phagocytosis. On the contrary, IgG-coated SiNPs stimulated the macrophage response, causing acceleration of nanoparticle internalization due to IgG interactions with macrophage Fc receptors. This finding establishes that simple and effective coating strategies can be devised not only to form protein adlayers on SiNP surfaces but also to endow protein-coated nanoparticles with important biological functions as demonstrated by both FH- and IgG-coated SiNPs. In an *in vivo* setting, we anticipate that a protein precoating on the nanoparticle surface may play a critical role in dictating the organization of the biomolecular corona, whereby the engineered protein precoating would replace the biological hard corona. Consequently, the protein precoating would influence the assembly of additional plasma protein layers constituting the soft corona and thus enable control over cellular interactions and related immune responses.[50,54,76] In addition, past studies have shown that it is possible to preserve the biological functions of proteins in the precoated adlayer on nanoparticle surfaces even after subsequent formation of the soft corona.[50,53,71] While the nanoparticle design in our study was simple and consisted of bulk SiNPs, the design principles and methods employed are broadly extendable to various classes of SiNPs, including silica-coated nanoparticles.[77−79] Indeed, there are many types of silica-coated nanoparticles that are routinely used in intravenous administration settings,[80−82] and establishing effective strategies to mitigate potential immunotoxicities such as CARPA effects is paramount. Together, our findings show that SiNPs can induce complement activation along the alternative pathway and protein coatings can mitigate SiNP-triggered complement activation and related adverse effects such as macrophage uptake. Looking forward, the protein coating strategy developed in this work and mechanistic insights into SiNP-triggered complement activation and mitigation thereof will be important for developing next-generation SiNPs for numerous

https://dx.doi.org/10.1021/acsnano.0c05097
ACS Nano 2020, 14, 11950−11961

applications and can be further explored for many types of inorganic nanoparticles.

MATERIALS AND METHODS

Reagents. Bovine serum albumin (A2153), human serum albumin (A3782), and human immunoglobulin G (I4506) were purchased from Sigma-Aldrich (St. Louis, MO, USA), and human fibrinogen (FIB3) was obtained from Enzyme Research Laboratories (South Bend, IN, USA). Purified complement components, including factor H (A137), factor I (A138), complement C3b (A114), and complement iC3b (A115), were procured from Complement Technology (Tyler, TX, USA) along with human blood serum (NHS), factor B-depleted serum (A335), MgEGTA (B106), and Zymosan (B400). The primary mouse monoclonal antibodies for C3b (MA140155) and iC3b (neoantigen) (MA182814) were obtained from Life Technologies (Singapore), and the secondary goat anti-mouse IgG-HRP conjugate (170−6516) was procured from Bio-Rad Laboratories (Singapore). Spherical, 100 nm diameter SiO_2 nanoparticles were obtained from NanoComposix (San Diego, CA, USA) and supplied at a concentration of 10 mg/mL in deionized water. FITC-labeled silica nanoparticles (100 nm diameter) were obtained from Nanocs Inc. (Boston, MA, USA) as a 1% suspension in aqueous solution. The murine macrophage cell line RAW 264.7 was obtained from ATCC (Old Town Manassas, VA, USA). All other reagents were purchased from Sigma-Aldrich and were of analytical grade.

Protein Coating. The as-supplied nanoparticles were centrifuged and resuspended in 10 mM Tris buffer solution with 150 mM NaCl at a nominal concentration of 1 mg/mL SiNPs. The samples were titrated with 1 M HCl to a final pH value of 7.5. Prior to the coating procedure, the protein solutions were freshly prepared in 10 mM Tris buffer [pH 7.5] with 150 mM NaCl at a nominal concentration of 2 mg/mL and diluted as appropriate in equivalent buffer. Then, 500 μL of SiNPs was incubated with 500 μL of the appropriate protein solution at 37 °C for 2 h. The samples were centrifuged at 16000*g* for 30 min, and 900 μL of the supernatant was replaced with fresh Tris buffer. This washing process was repeated twice (three times in total), and the supernatant after each washing step was analyzed to verify that there was a negligible amount of free protein in the final protein-coated nanoparticle suspension.

Nanoparticle Size Characterization. The hydrodynamic diameter of pristine and protein-coated SiNPs was evaluated by DLS and NTA. A NanoBrook 90Plus particle size analyzer (Brookhaven Instruments, Holtsville, NY, USA) was used to characterize the intensity-weighted SiNP size distribution. As part of the coating process, SiNPs were characterized prior to incubation, immediately after incubation, and after completion of the washing protocol. All measurements were performed with a 658.0 nm monochromatic laser, and the mean hydrodynamic diameter is reported from n = 5 measurements. Size characterization by NTA experiments was conducted using a NanoSight LM10 instrument (Malvern Instruments, Malvern, UK) in order to measure the number-weighted size distribution of SiNPs before and after protein coating. The NTA measurements (n = 3) were performed using a laser with 405 nm wavelength, and a built-in sCMOS camera recorded the nanoparticle-scattered light for a total period of 3 min at a rate of 25 frames per second.

Quantification of Protein Coating. The amount of protein bound to SiNPs was quantified by a bicinchoninic acid protein assay from Thermo Fisher Scientific (Pierce BCA protein assay kit, catalog no. 23225). After coating the SiNPs, the sample was centrifuged at 16000*g* for 30 min, and 950 μL of the supernatant (including unbound protein) was transferred to a separate vial. The remaining 50 μL of solution containing the protein−SiNP pellet and 50 μL of the supernatant were resuspended with 400 μL of BCA working reagent and incubated at 37 °C for 2 h. The light absorbance intensity at 562 nm wavelength was measured in triplicate for each sample with a Tecan Infinite M200 Pro microplate reader (Tecan, Männedorf, Switzerland), and the protein concentrations were determined according to the manufacturer's instructions. The SiNP-bound protein concentration was determined by calculating the difference of the supernatant and background measurements from the pellet sample measurement. The final values are reported as protein mass per mg SiNP.

Complement Activation Assays. The concentrations of complement proteins produced due to complement activation were quantified by ELISA using the MicroVue SC5b-9 Plus EIA (A020), MicroVue C3a Plus EIA (A031), MicroVue Bb Plus EIA (A027), and MicroVue C4a EIA (A035) kits supplied by Quidel (San Diego, CA, USA). Prior to measurements, protein-coated SiNP solutions were centrifuged and the supernatants were discarded. The remaining pellets were resuspended and incubated with fresh human serum at a 1:4 volumetric ratio at 37 °C for 30 min and then transferred to an ice bath followed by the addition of EDTA-containing buffer to each vial to cease further complement activation. Heat-treated IgG (prepared at 70 °C for 30 min) was used as the positive control, and normal human serum without SiNPs served as the negative control. All samples were measured in triplicate in three independent experiments for a total of 9 experiments per sample (n = 9) and were handled in accordance with the manufacturer's instructions, and the results were reported as the mean and standard deviation.

SDS-PAGE and Western Blot Analysis. A 500 μL aliquot of protein-coated SiNPs was mixed with 500 μL of purified C3b (0.05 mg/mL) in the presence or absence of 50 μL of purified factor I (0.05 mg/mL). The mixture was incubated at 37 °C for 30 min and then centrifuged at 16000*g* for 30 min; the supernatant of each sample was collected for analysis. The samples were mixed with a 4× loading buffer (4× Laemmli sample buffer containing 10% β-ME (2-mercaptoethanol)), boiled for 5 min, and then centrifuged for 1 min at 16000*g*. Then, 10 μL of each sample along with a protein standard marker (Precision Plus Kaleidoscope Prestained Protein Standards) was loaded into the wells of an 8% polyacrylamide gel, and electrophoresis was conducted at 50 V for 15 min, followed by 100 V for another 1.5 h. The processed gels were trans-blotted onto a nitrocellulose membrane at 300 mA for 2 h, and the blots were briefly rinsed with deionized water prior to blocking in TBST (Tris buffer, pH 7.6, with 0.5% Tween-20) containing 3% BSA for 1 h at room temperature with gentle agitation. The blots were then incubated with primary antibodies of C3b or iC3b (diluted 1:500 in blocking buffer) at 4 °C overnight, followed by three washing cycles with TBST. Subsequently, the membranes were incubated with horseradish peroxide-conjugated secondary antibody (diluted 1:2000 in blocking buffer) for 1 h at room temperature and rinsed four times with TBST. The HRP labels on the proteins were detected with the addition of an enhanced chemiluminescent substrate, and the resulting bands were imaged with an Amersham Imager 600 chemiluminescence imager (GE Healthcare, Chicago, IL, USA).

Nanoparticle Uptake. RAW 264.7 cells were cultured in Dulbecco's modified Eagle medium (DMEM) containing 4.5 g/L D-glucose, L-glutamine, and 110 mg/L sodium pyruvate (Gibco), supplemented with 10% FBS (HyClone, GE Healthcare) and 1% streptomycin/amphotericin B/penicillin (Anti-Anti; Gibco, Thermo Fisher Scientific, Waltham, MA, USA), at 37 °C in a 5% CO_2 environment. For the uptake experiments, cells were seeded at a density of 35 000 cells/cm. On the following day, the cells were incubated in fresh serum-free medium for 2 h, before protein-coated or bare nanoparticles dispersed in serum-free medium were added at a concentration of 80 μg/mL. The cells were incubated for 150 min in normal growth conditions and then washed thoroughly with ice-cold PBS (Gibco).

Flow Cytometry Analysis. After incubation with the SiNP samples, the RAW 264.7 cells were detached from the culture vessel with 2.5% trypsin (Gibco) and kept on ice. To measure the fluorescence intensity of internally localized nanoparticles, cells were incubated for 2 min with an equal volume of 0.4% TB solution (Sigma-Aldrich) and analyzed immediately afterward. Flow cytometry measurements were performed on a BD LSRFortessa X-20 cytometer (BD Biosciences, Franklin Lakes, NJ, USA), using a blue laser for excitation and a 525/50 nm bandpass filter for emission detection. Data analysis was performed using the FCS Express 6 software

https://dx.doi.org/10.1021/acsnano.0c05097
ACS Nano 2020, 14, 11950−11961

package (DeNovo Software, Pasadena, CA, USA). Single, viable cells were selected, and the gated events were further analyzed by the amount of fluorescent signal expressed as the median intensity.

Confocal Microscopy Imaging. After incubation with fluorescently labeled SiNP samples, RAW 264.7 cellular membranes were stained with CellMask Orange (Invitrogen, Carlsbad, CA, USA), according to the manufacturer's protocol. Then, the cells were fixed with 4% paraformaldehyde solution (Life Technologies, Carlsbad, CA, USA) at 37 °C for 10 min. For staining of cell nuclei, fixed cells were incubated with Hoechst 33342 (Invitrogen), following the manufacturer's protocol. Images were taken with an LSM 710 microscope (Carl Zeiss, Oberkochen, Germany), using an EC Plan-Neofluar 100×/1.3 oil M27 objective. Fluorescent nanoparticles were excited with a 488 nm argon laser, and emission was detected in the wavelength range of 493 to 556 nm. The fluorescence of cell membranes was excited with a 561 nm DPSS laser, and emission was detected in the wavelength range of 566 to 681 nm. The fluorescence of cell nuclei was excited with a 405 nm diode laser and detected in the wavelength range of 410 to 483 nm.

ASSOCIATED CONTENT

Supporting Information

The Supporting Information is available free of charge at https://pubs.acs.org/doi/10.1021/acsnano.0c05097.

Size measurements by DLS of SiNPs before and after protein coating, murine macrophage uptake study reference list, flow cytometric analyses of FITC profile in macrophages, CLSM image with orthogonal view of cells, and cytometric analyses of SiNP uptake with and without TB treatment (PDF)

AUTHOR INFORMATION

Corresponding Authors

Nam-Joon Cho − *School of Materials Science and Engineering, Nanyang Technological University, Singapore 639798 Singapore; SKKU-UCLA-NTU Precision Biology Research Center, Sungkyunkwan University, Suwon 16419, Republic of Korea;* orcid.org/0000-0002-8692-8955; Email: njcho@ntu.edu.sg

Paul S. Weiss − *Department of Chemistry and Biochemistry and California NanoSystems Institute and Department of Bioengineering and Department of Materials Science and Engineering, University of California, Los Angeles, Los Angeles, California 90095, United States; SKKU-UCLA-NTU Precision Biology Research Center, Sungkyunkwan University, Suwon 16419, Republic of Korea;* orcid.org/0000-0001-5527-6248; Email: psw@cnsi.ucla.edu

Authors

Jae Hyeon Park − *School of Materials Science and Engineering, Nanyang Technological University, Singapore 639798 Singapore; Department of Chemistry and Biochemistry and California NanoSystems Institute, University of California, Los Angeles, Los Angeles, California 90095, United States;* orcid.org/0000-0002-2266-943X

Joshua A. Jackman − *School of Chemical Engineering and SKKU-UCLA-NTU Precision Biology Research Center, Sungkyunkwan University, Suwon 16419, Republic of Korea;* orcid.org/0000-0002-1800-8102

Abdul Rahim Ferhan − *School of Materials Science and Engineering, Nanyang Technological University, Singapore 639798 Singapore;* orcid.org/0000-0003-3238-3125

Jason N. Belling − *Department of Chemistry and Biochemistry and California NanoSystems Institute, University of California, Los Angeles, Los Angeles, California 90095, United States;* orcid.org/0000-0001-7750-5689

Natalia Mokrzecka − *School of Materials Science and Engineering, Nanyang Technological University, Singapore 639798 Singapore*

Complete contact information is available at: https://pubs.acs.org/10.1021/acsnano.0c05097

Author Contributions

JHP, JAJ, PSW, and NJC designed the study and experimental plans. JHP and JNB prepared samples and conducted the ELISA and Western Blot experiments. NM prepared the cell cultures and performed the nanoparticle uptake and FCM experiments. JHP, JAJ, ARF, and JNB analyzed the data. JHP and JAJ prepared the manuscript draft, and all authors reviewed and approved the final draft.

Notes

The authors declare no competing financial interest.

ACKNOWLEDGMENTS

N.J.C. acknowledges support from the National Research Foundation of Singapore through a Competitive Research Programme grant (NRF-CRP10-2012-07) as well as from Nanyang Technological University through a start-up grant (M4080751.070). J.A.J. acknowledges support from the National Research Foundation of Korea (NRF) grant funded by the Korean government (MSIT) (No. 2020R1C1C1004385). J.N.B. thanks the NIH for a predoctoral fellowship; research reported in this publication was supported by the National Heart, Lung, and Blood Institute of the National Institutes of Health under Award Number F31HL149356.

REFERENCES

(1) Tang, L.; Cheng, J. Nonporous Silica Nanoparticles for Nanomedicine Application. *Nano Today* **2013**, *8*, 290−312.

(2) Barbe, C.; Bartlett, J.; Kong, L. G.; Finnie, K.; Lin, H. Q.; Larkin, M.; Calleja, S.; Bush, A.; Calleja, G. Silica Particles: A Novel Drug-Delivery System. *Adv. Mater.* **2004**, *16*, 1959−1966.

(3) Gimenez, C.; de la Torre, C.; Gorbe, M.; Aznar, E.; Sancenon, F.; Murguia, J. R.; Martinez-Manez, R.; Marcos, M. D.; Amoros, P. Gated Mesoporous Silica Nanoparticles for the Controlled Delivery of Drugs in Cancer Cells. *Langmuir* **2015**, *31*, 3753−3762.

(4) Liberman, A.; Mendez, N.; Trogler, W. C.; Kummel, A. C. Synthesis and Surface Functionalization of Silica Nanoparticles for Nanomedicine. *Surf. Sci. Rep.* **2014**, *69*, 132−158.

(5) Fruijtier-Polloth, C. The Toxicological Mode of Action and the Safety of Synthetic Amorphous Silica-A Nanostructured Material. *Toxicology* **2012**, *294*, 61−79.

(6) Lehman, S. E.; Mudunkotuwa, I. A.; Grassian, V. H.; Larsen, S. C. Nano-Bio Interactions of Porous and Nonporous Silica Nanoparticles of Varied Surface Chemistry: A Structural, Kinetic, and Thermodynamic Study of Protein Adsorption from RPMI Culture Medium. *Langmuir* **2016**, *32*, 731−742.

(7) Pelaz, B.; Alexiou, C.; Alvarez-Puebla, R. A.; Alves, F.; Andrews, A. M.; Ashraf, S.; Balogh, L. P.; Ballerini, L.; Bestetti, A.; Brendel, C.; Bosi, S.; Carril, M.; Chan, W. C.; Chen, C.; Chen, X.; Chen, X.; Cheng, Z.; Cui, D.; Du, J.; Dullin, C.; et al. Diverse Applications of Nanomedicine. *ACS Nano* **2017**, *11*, 2313−2381.

(8) Tarn, D.; Ashley, C. E.; Xue, M.; Carnes, E. C.; Zink, J. I.; Brinker, C. J. Mesoporous Silica Nanoparticle Nanocarriers: Biofunctionality and Biocompatibility. *Acc. Chem. Res.* **2013**, *46*, 792−801.

(9) Contado, C.; Mejia, J.; Lozano Garcia, O.; Piret, J. P.; Dumortier, E.; Toussaint, O.; Lucas, S. Physicochemical and

Toxicological Evaluation of Silica Nanoparticles Suitable for Food and Consumer Products Collected by Following the EC Recommendation. *Anal. Bioanal. Chem.* **2016**, *408*, 271−286.
(10) Dekkers, S.; Krystek, P.; Peters, R. J.; Lankveld, D. P.; Bokkers, B. G.; van Hoeven-Arentzen, P. H.; Bouwmeester, H.; Oomen, A. G. Presence and Risks of Nanosilica in Food Products. *Nanotoxicology* **2011**, *5*, 393−405.
(11) Wang, M.; Tian, J.; Zhang, H.; Shi, X.; Chen, Z.; Wang, Y.; Ji, A.; Gao, Y. Novel Synthesis of Pure VO_2@SiO_2 Core@Shell Nanoparticles to Improve the Optical and Anti-Oxidant Properties of a VO_2 Film. *RSC Adv.* **2016**, *6*, 108286−108289.
(12) Zhong, Q.; Cao, M.; Hu, H.; Yang, D.; Chen, M.; Li, P.; Wu, L.; Zhang, Q. One-Pot Synthesis of Highly Stable $CsPbBr_3$@SiO_2 Core-Shell Nanoparticles. *ACS Nano* **2018**, *12*, 8579−8587.
(13) Hu, G.; Yang, L.; Li, Y.; Wang, L. Continuous and Scalable Fabrication of Stable and Biocompatible MOF@SiO_2 Nanoparticles for Drug Loading. *J. Mater. Chem. B* **2018**, *6*, 7936−7942.
(14) Foglia, S.; Ledda, M.; Fioretti, D.; Iucci, G.; Papi, M.; Capellini, G.; Lolli, M. G.; Grimaldi, S.; Rinaldi, M.; Lisi, A. *In Vitro* Biocompatibility Study of Sub-5 nm Silica-Coated Magnetic Iron Oxide Fluorescent Nanoparticles for Potential Biomedical Application. *Sci. Rep.* **2017**, *7*, 46513.
(15) Ruan, J.; Wang, K.; Song, H.; Xu, X.; Ji, J.; Cui, D. Biocompatibility of Hydrophilic Silica-Coated CdTe Quantum Dots and Magnetic Nanoparticles. *Nanoscale Res. Lett.* **2011**, *6*, 299.
(16) Gerion, D.; Pinaud, F.; Williams, S. C.; Parak, W. J.; Zanchet, D.; Weiss, S.; Alivisatos, A. P. Synthesis and Properties of Biocompatible Water-Soluble Silica-Coated CdSe/ZnS Semiconductor Quantum Dots. *J. Phys. Chem. B* **2001**, *105*, 8861−8871.
(17) Malvindi, M. A.; De Matteis, V.; Galeone, A.; Brunetti, V.; Anyfantis, G. C.; Athanassiou, A.; Cingolani, R.; Pompa, P. P. Toxicity Assessment of Silica Coated Iron Oxide Nanoparticles and Biocompatibility Improvement by Surface Engineering. *PLoS One* **2014**, *9*, No. e85835.
(18) Jia, L.; Kitamoto, Y. Influence of Silica Coating Process on Fine Structure and Magnetic Properties of Iron Oxide Nanoparticles. *Electrochim. Acta* **2015**, *183*, 148−152.
(19) Kunzmann, A.; Andersson, B.; Vogt, C.; Feliu, N.; Ye, F.; Gabrielsson, S.; Toprak, M. S.; Buerki-Thurnherr, T.; Laurent, S.; Vahter, M.; Krug, H.; Muhammed, M.; Scheynius, A.; Fadeel, B. Efficient Internalization of Silica-Coated Iron Oxide Nanoparticles of Different Sizes by Primary Human Macrophages and Dendritic Cells. *Toxicol. Appl. Pharmacol.* **2011**, *253*, 81−93.
(20) Dobrovolskaia, M. A.; McNeil, S. E. Immunological Properties of Engineered Nanomaterials. *Nat. Nanotechnol.* **2007**, *2*, 469−478.
(21) Lehman, S. E.; Morris, A. S.; Mueller, P. S.; Salem, A. K.; Grassian, V. H.; Larsen, S. C. Silica Nanoparticle-Generated ROS as a Predictor of Cellular Toxicity: Mechanistic Insights and Safety by Design. *Environ. Sci.: Nano* **2016**, *3*, 56−66.
(22) Nel, A.; Xia, T.; Madler, L.; Li, N. Toxic Potential of Materials at the Nanolevel. *Science* **2006**, *311*, 622−627.
(23) Yu, T.; Malugin, A.; Ghandehari, H. Impact of Silica Nanoparticle Design on Cellular Toxicity and Hemolytic Activity. *ACS Nano* **2011**, *5*, 5717−5728.
(24) Saikia, J.; Yazdimamaghani, M.; Hadipour Moghaddam, S. P.; Ghandehari, H. Differential Protein Adsorption and Cellular Uptake of Silica Nanoparticles Based on Size and Porosity. *ACS Appl. Mater. Interfaces* **2016**, *8*, 34820−34832.
(25) Bottazzi, B.; Doni, A.; Garlanda, C.; Mantovani, A. An Integrated View of Humoral Innate Immunity: Pentraxins as a Paradigm. *Annu. Rev. Immunol.* **2010**, *28*, 157−183.
(26) Ricklin, D.; Hajishengallis, G.; Yang, K.; Lambris, J. D. Complement: A Key System for Immune Surveillance and Homeostasis. *Nat. Immunol.* **2010**, *11*, 785−797.
(27) Zolnik, B. S.; Gonzalez-Fernandez, A.; Sadrieh, N.; Dobrovolskaia, M. A. Nanoparticles and the Immune System. *Endocrinology* **2010**, *151*, 458−465.
(28) Pio, R.; Corrales, L.; Lambris, J. D. The Role of Complement in Tumor Growth. *Adv. Exp. Med. Biol.* **2014**, *772*, 229−262.
(29) Trouw, L. A.; Blom, A. M.; Gasque, P. Role of Complement and Complement Regulators in the Removal of Apoptotic Cells. *Mol. Immunol.* **2008**, *45*, 1199−1207.
(30) Szebeni, J. Complement Activation-Related Pseudoallergy: A Stress Reaction in Blood Triggered by Nanomedicines and Biologicals. *Mol. Immunol.* **2014**, *61*, 163−173.
(31) Klos, A.; Tenner, A. J.; Johswich, K. O.; Ager, R. R.; Reis, E. S.; Kohl, J. The Role of the Anaphylatoxins in Health and Disease. *Mol. Immunol.* **2009**, *46*, 2753−2766.
(32) La-Beck, N. M.; Gabizon, A. A. Nanoparticle Interactions with the Immune System: Clinical Implications for Liposome-Based Cancer Chemotherapy. *Front. Immunol.* **2017**, *8*, 416.
(33) Xing, G. Q.; Chen, M.; Liu, G.; Heeringa, P.; Zhang, J. J.; Zheng, X.; E, J.; Kallenberg, C. G.; Zhao, M. H. Complement Activation Is Involved in Renal Damage in Human Antineutrophil Cytoplasmic Autoantibody Associated Pauci-Immune Vasculitis. *J. Clin. Immunol.* **2009**, *29*, 282−291.
(34) Pelaz, B.; del Pino, P.; Maffre, P.; Hartmann, R.; Gallego, M.; Rivera-Fernandez, S.; de la Fuente, J. M.; Nienhaus, G. U.; Parak, W. J. Surface Functionalization of Nanoparticles with Polyethylene Glycol: Effects on Protein Adsorption and Cellular Uptake. *ACS Nano* **2015**, *9*, 6996−7008.
(35) Harris, J. M.; Chess, R. B. Effect of PEGylation on Pharmaceuticals. *Nat. Rev. Drug Discovery* **2003**, *2*, 214−221.
(36) Perry, J. L.; Reuter, K. G.; Kai, M. P.; Herlihy, K. P.; Jones, S. W.; Luft, J. C.; Napier, M.; Bear, J. E.; DeSimone, J. M. PEGylated PRINT Nanoparticles: The Impact of PEG Density on Protein Binding, Macrophage Association, Biodistribution, and Pharmacokinetics. *Nano Lett.* **2012**, *12*, 5304−5310.
(37) Walkey, C. D.; Chan, W. C. Understanding and Controlling the Interaction of Nanomaterials with Proteins in a Physiological Environment. *Chem. Soc. Rev.* **2012**, *41*, 2780−2799.
(38) Adamiak, L.; Touve, M. A.; LeGuyader, C. L. M.; Gianneschi, N. C. Peptide Brush Polymers and Nanoparticles with Enzyme-Regulated Structure and Charge for Inducing or Evading Macrophage Cell Uptake. *ACS Nano* **2017**, *11*, 9877−9888.
(39) He, Q.; Zhang, J.; Shi, J.; Zhu, Z.; Zhang, L.; Bu, W.; Guo, L.; Chen, Y. The Effect of PEGylation of Mesoporous Silica Nanoparticles on Nonspecific Binding of Serum Proteins and Cellular Responses. *Biomaterials* **2010**, *31*, 1085−1092.
(40) Hamad, I.; Hunter, A. C.; Szebeni, J.; Moghimi, S. M. Poly(ethylene Glycol)s Generate Complement Activation Products in Human Serum through Increased Alternative Pathway Turnover and a MASP-2-Dependent Process. *Mol. Immunol.* **2008**, *46*, 225−232.
(41) Yang, Q.; Lai, S. K. Anti-PEG Immunity: Emergence, Characteristics, and Unaddressed Questions. *Wiley Interdiscip Rev. Nanomed Nanobiotechnol* **2015**, *7*, 655−677.
(42) Ganson, N. J.; Povsic, T. J.; Sullenger, B. A.; Alexander, J. H.; Zelenkofske, S. L.; Sailstad, J. M.; Rusconi, C. P.; Hershfield, M. S. Pre-Existing Anti-Polyethylene Glycol Antibody Linked to First-Exposure Allergic Reactions to Pegnivacogin, A PEGylated RNA Aptamer. *J. Allergy Clin. Immunol.* **2016**, *137*, 1610−1613.
(43) Knop, K.; Hoogenboom, R.; Fischer, D.; Schubert, U. S. Poly(ethylene Glycol) in Drug Delivery: Pros and Cons as well as Potential Alternatives. *Angew. Chem., Int. Ed.* **2010**, *49*, 6288−6308.
(44) Hu, C. M.; Zhang, L.; Aryal, S.; Cheung, C.; Fang, R. H.; Zhang, L. Erythrocyte Membrane-Camouflaged Polymeric Nanoparticles as a Biomimetic Delivery Platform. *Proc. Natl. Acad. Sci. U. S. A.* **2011**, *108*, 10980−10985.
(45) Belling, J. N.; Jackman, J. A.; Yorulmaz Avsar, S.; Park, J. H.; Wang, Y.; Potroz, M. G.; Ferhan, A. R.; Weiss, P. S.; Cho, N. J. Stealth Immune Properties of Graphene Oxide Enabled by Surface-Bound Complement Factor H. *ACS Nano* **2016**, *10*, 10161−10172.
(46) Li, Y.; Qiu, W.; Zhang, L.; Fung, J.; Lin, F. Painting Factor H onto Mesenchymal Stem Cells Protects the Cells from Complement- and Neutrophil-Mediated Damage. *Biomaterials* **2016**, *102*, 209−219.
(47) Lu, X.; Xu, P.; Ding, H. M.; Yu, Y. S.; Huo, D.; Ma, Y. Q. Tailoring the Component of Protein Corona *via* Simple Chemistry. *Nat. Commun.* **2019**, *10*, 4520.

https://dx.doi.org/10.1021/acsnano.0c05097
ACS Nano 2020, 14, 11950−11961

(48) Ogawara, K.; Furumoto, K.; Nagayama, S.; Minato, K.; Higaki, K.; Kai, T.; Kimura, T. Pre-Coating with Serum Albumin Reduces Receptor-Mediated Hepatic Disposition of Polystyrene Nanosphere: Implications for Rational Design of Nanoparticles. *J. Controlled Release* **2004**, *100*, 451−455.
(49) Peng, Q.; Zhang, S.; Yang, Q.; Zhang, T.; Wei, X. Q.; Jiang, L.; Zhang, C. L.; Chen, Q. M.; Zhang, Z. R.; Lin, Y. F. Preformed Albumin Corona, A Protective Coating for Nanoparticles Based Drug Delivery System. *Biomaterials* **2013**, *34*, 8521−8530.
(50) Schottler, S.; Becker, G.; Winzen, S.; Steinbach, T.; Mohr, K.; Landfester, K.; Mailander, V.; Wurm, F. R. Protein Adsorption Is Required for Stealth Effect of Poly(ethylene Glycol)- and Poly-(phosphoester)-Coated Nanocarriers. *Nat. Nanotechnol.* **2016**, *11*, 372−377.
(51) Ke, P. C.; Lin, S.; Parak, W. J.; Davis, T. P.; Caruso, F. A Decade of the Protein Corona. *ACS Nano* **2017**, *11*, 11773−11776.
(52) Walkey, C. D.; Olsen, J. B.; Song, F.; Liu, R.; Guo, H.; Olsen, D. W.; Cohen, Y.; Emili, A.; Chan, W. C. Protein Corona Fingerprinting Predicts the Cellular Interaction of Gold and Silver Nanoparticles. *ACS Nano* **2014**, *8*, 2439−2455.
(53) Tonigold, M.; Simon, J.; Estupinan, D.; Kokkinopoulou, M.; Reinholz, J.; Kintzel, U.; Kaltbeitzel, A.; Renz, P.; Domogalla, M. P.; Steinbrink, K.; Lieberwirth, I.; Crespy, D.; Landfester, K.; Mailander, V. Pre-Adsorption of Antibodies Enables Targeting of Nanocarriers Despite a Biomolecular Corona. *Nat. Nanotechnol.* **2018**, *13*, 862−869.
(54) Simon, J.; Muller, L. K.; Kokkinopoulou, M.; Lieberwirth, I.; Morsbach, S.; Landfester, K.; Mailander, V. Exploiting the Biomolecular Corona: Pre-Coating of Nanoparticles Enables Controlled Cellular Interactions. *Nanoscale* **2018**, *10*, 10731−10739.
(55) Park, J. H.; Sut, T. N.; Jackman, J. A.; Ferhan, A. R.; Yoon, B. K.; Cho, N. J. Controlling Adsorption and Passivation Properties of Bovine Serum Albumin on Silica Surfaces by Ionic Strength Modulation and Cross-Linking. *Phys. Chem. Chem. Phys.* **2017**, *19*, 8854−8865.
(56) Park, J. H.; Jackman, J. A.; Ferhan, A. R.; Ma, G. J.; Yoon, B. K.; Cho, N. J. Temperature-Induced Denaturation of BSA Protein Molecules for Improved Surface Passivation Coatings. *ACS Appl. Mater. Interfaces* **2018**, *10*, 32047−32057.
(57) Yu, C. H.; Al-Saadi, A.; Shih, S.-J.; Qiu, L.; Tam, K. Y.; Tsang, S. C. Immobilization of BSA on Silica-Coated Magnetic Iron Oxide Nanoparticle. *J. Phys. Chem. C* **2009**, *113*, 537−543.
(58) Zhu, J.; Sun, Z.; Li, J. J.; Zhao, J. W. Bovine Serum Albumins (BSA) Induced Aggregation and Separation of Gold Colloid Nanoparticles. *J. Nanosci. Nanotechnol.* **2012**, *12*, 2206−2211.
(59) Ho, Y. T.; Azman, N.; Loh, F. W. Y.; Ong, G. K. T.; Engudar, G.; Kriz, S. A.; Kah, J. C. Y. Protein Corona Formed from Different Blood Plasma Proteins Affects the Colloidal Stability of Nanoparticles Differently. *Bioconjugate Chem.* **2018**, *29*, 3923−3934.
(60) Kim, A.; Ng, W. B.; Bernt, W.; Cho, N. J. Validation of Size Estimation of Nanoparticle Tracking Analysis on Polydisperse Macromolecule Assembly. *Sci. Rep.* **2019**, *9*, 2639.
(61) Filipe, V.; Hawe, A.; Jiskoot, W. Critical Evaluation of Nanoparticle Tracking Analysis (NTA) by NanoSight for the Measurement of Nanoparticles and Protein Aggregates. *Pharm. Res.* **2010**, *27*, 796−810.
(62) Cukalevski, R.; Ferreira, S. A.; Dunning, C. J.; Berggård, T.; Cedervall, T. IgG and Fibrinogen Driven Nanoparticle Aggregation. *Nano Res.* **2015**, *8*, 2733−2743.
(63) Mortensen, S. A.; Sander, B.; Jensen, R. K.; Pedersen, J. S.; Golas, M. M.; Jensenius, J. C.; Hansen, A. G.; Thiel, S.; Andersen, G. R. Structure and Activation of C1, the Complex Initiating the Classical Pathway of the Complement Cascade. *Proc. Natl. Acad. Sci. U. S. A.* **2017**, *114*, 986−991.
(64) Kocsis, A.; Kekesi, K. A.; Szasz, R.; Vegh, B. M.; Balczer, J.; Dobo, J.; Zavodszky, P.; Gal, P.; Pal, G. Selective Inhibition of the Lectin Pathway of Complement with Phage Display Selected Peptides Against Mannose-Binding Lectin-Associated Serine Protease (MASP)-1 and −2: Significant Contribution of MASP-1 to Lectin Pathway Activation. *J. Immunol.* **2010**, *185*, 4169−4178.
(65) Berger, M.; Broxup, B.; Sefton, M. V. Using ELISA to Evaluate Complement Activation by Reference Biomaterials. *J. Mater. Sci.: Mater. Med.* **1994**, *5*, 622−627.
(66) Wu, J.; Wu, Y. Q.; Ricklin, D.; Janssen, B. J.; Lambris, J. D.; Gros, P. Structure of Complement Fragment C3b-Factor H and Implications for Host Protection by Complement Regulators. *Nat. Immunol.* **2009**, *10*, 728−733.
(67) Gal, P.; Dobo, J.; Zavodszky, P.; Sim, R. B. Early Complement Proteases: C1r, C1s and MASPs. A Structural Insight into Activation and Functions. *Mol. Immunol.* **2009**, *46*, 2745−2752.
(68) Dunkelberger, J. R.; Song, W. C. Complement and its Role in Innate and Adaptive Immune Responses. *Cell Res.* **2010**, *20*, 34−50.
(69) Carlsson, F.; Sandin, C.; Lindahl, G. Human Fibrinogen Bound to *Streptococcus pyogenes* M Protein Inhibits Complement Deposition *via* the Classical Pathway. *Mol. Microbiol.* **2005**, *56*, 28−39.
(70) Vogler, E. A. Protein Adsorption in Three Dimensions. *Biomaterials* **2012**, *33*, 1201−1237.
(71) Herbert, A. P.; Makou, E.; Chen, Z. A.; Kerr, H.; Richards, A.; Rappsilber, J.; Barlow, P. N. Complement Evasion Mediated by Enhancement of Captured Factor H: Implications for Protection of Self-Surfaces from Complement. *J. Immunol.* **2015**, *195*, 4986−4998.
(72) Gustafson, H. H.; Holt-Casper, D.; Grainger, D. W.; Ghandehari, H. Nanoparticle Uptake: The Phagocyte Problem. *Nano Today* **2015**, *10*, 487−510.
(73) van Lookeren Campagne, M.; Wiesmann, C.; Brown, E. J. Macrophage Complement Receptors and Pathogen Clearance. *Cell. Microbiol.* **2007**, *9*, 2095−2102.
(74) Lesniak, A.; Fenaroli, F.; Monopoli, M. P.; Aberg, C.; Dawson, K. A.; Salvati, A. Effects of the Presence or Absence of a Protein Corona on Silica Nanoparticle Uptake and Impact on Cells. *ACS Nano* **2012**, *6*, 5845−5857.
(75) Mirshafiee, V.; Kim, R.; Park, S.; Mahmoudi, M.; Kraft, M. L. Impact of Protein Pre-Coating on the Protein Corona Composition and Nanoparticle Cellular Uptake. *Biomaterials* **2016**, *75*, 295−304.
(76) Ritz, S.; Schottler, S.; Kotman, N.; Baier, G.; Musyanovych, A.; Kuharev, J.; Landfester, K.; Schild, H.; Jahn, O.; Tenzer, S.; Mailander, V. Protein Corona of Nanoparticles: Distinct Proteins Regulate the Cellular Uptake. *Biomacromolecules* **2015**, *16*, 1311−1321.
(77) Möller, K.; Bein, T. Degradable Drug Carriers: Vanishing Mesoporous Silica Nanoparticles. *Chem. Mater.* **2019**, *31*, 4364−4378.
(78) Hristov, D.; McCartney, F.; Beirne, J.; Mahon, E.; Reid, S.; Bhattacharjee, S.; Penarier, G.; Werner, U.; Bazile, D.; Brayden, D. J. Silica-Coated Nanoparticles with a Core of Zinc, l-Arginine, and a Peptide Designed for Oral Delivery. *ACS Appl. Mater. Interfaces* **2020**, *12*, 1257−1269.
(79) Ledda, M.; Fioretti, D.; Lolli, M. G.; Papi, M.; Di Gioia, C.; Carletti, R.; Ciasca, G.; Foglia, S.; Palmieri, V.; Marchese, R.; Grimaldi, S.; Rinaldi, M.; Lisi, A. Biocompatibility Assessment of Sub-5 nm Silica-Coated Superparamagnetic Iron Oxide Nanoparticles in Human Stem Cells and in Mice for Potential Application in Nanomedicine. *Nanoscale* **2020**, *12*, 1759−1778.
(80) Waegeneers, N.; Brasseur, A.; Van Doren, E.; Van der Heyden, S.; Serreyn, P. J.; Pussemier, L.; Mast, J.; Schneider, Y. J.; Ruttens, A.; Roels, S. Short-Term Biodistribution and Clearance of Intravenously Administered Silica Nanoparticles. *Toxicol. Rep.* **2018**, *5*, 632−638.
(81) Zhou, M.; Ge, X.; Ke, D. M.; Tang, H.; Zhang, J. Z.; Calvaresi, M.; Gao, B.; Sun, L.; Su, Q.; Wang, H. The Bioavailability, Biodistribution, and Toxic Effects of Silica-Coated Upconversion Nanoparticles *In Vivo*. *Front. Chem.* **2019**, *7*, 218.
(82) Dogra, P.; Adolphi, N. L.; Wang, Z.; Lin, Y. S.; Butler, K. S.; Durfee, P. N.; Croissant, J. G.; Noureddine, A.; Coker, E. N.; Bearer, E. L.; Cristini, V.; Brinker, C. J. Establishing the Effects of Mesoporous Silica Nanoparticle Properties on *In Vivo* Disposition Using Imaging-based Pharmacokinetics. *Nat. Commun.* **2018**, *9*, 4551.

https://dx.doi.org/10.1021/acsnano.0c05097
ACS Nano 2020, 14, 11950−11961